Solid State Ionics 292 (2016) 103–109

Contents lists available at ScienceDirect

Solid State Ionics

journal homepage: www.elsevier.com/locate/ssi

Raman and XRD studies on the influence of nano silicon surface modification on Li^+ dynamics processes of $LiFePO_4$

Wenyu Yang, Mingzhong Zou, Guiying Zhao, Zhensheng Hong, Qian Feng, Jiaxin Li, Yingbin Lin, Zhigao Huang *

[a] Fujian Provincial Key Laboratory of Quantum Manipulation and New Energy Materials, College of Physics and Energy, Fujian Normal University, Fuzhou 350117, China
[b] Fujian Provincial Collaborative Innovation Center for Optoelectronic Semiconductors and Efficient Devices, Xiamen 361005, China

ARTICLE INFO

Article history:
Received 24 November 2015
Received in revised form 18 May 2016
Accepted 28 May 2016
Available online xxxx

Keywords:
$LiFePO_4$
Surface modification
Li^+ dynamics
XRD
Raman

ABSTRACT

In this letter, Li^+ ion kinetic processes of $LiFePO_4$@C and $LiFePO_4$@C modified by nano silicon ($LiFePO_4$@C/Si) have been systematically investigated by X-ray diffraction, Raman spectra and Electrochemical impedance spectroscopy (EIS), respectively. The experimental results indicate that, (1) $LiFePO_4$@C/Si possesses faster charged and discharged velocity than $LiFePO_4$@C; (2) the nano silicon surface modification induces the larger diffusion coefficient and less activation energy of Li ions, which promotes Li^+ ion transfer rate; (3) it suppresses effectively the Fe dissolution and enhances the stability of $LiFePO_4$ phase and cycle performance; (4) there exists the best silicon surface modification content (Si content = 2.46 at.%) in enhancing the electrochemical performances of $LiFePO_4$. Additionally, it is suggested that constant-voltage charge is with some time indispensable for a fully delithiation of the $LiFePO_4$ material.

1. Introduction

Since the pioneering work in 1997 published by Padhi et al., lithium iron phosphate $LiFePO_4$ has become the most promising positive-electrode materials for the next generation of lithium-ion batteries due to its remarkable thermal stability, relatively high theoretical specific capacity of 170 mA h/g and flat charge-discharge profile at about 3.4 V vs. Li^+/Li [1,2]. However, the low electrical conductivity and slow lithium ion diffusion hindered its wide applications in the stored energy. In order to improve the electrochemical performances of $LiFePO_4$, many efforts have been made to increase the conductivity of $LiFePO_4$ by coating with electronic conducting agents [3–7], doping with metal and nonmetal ions [8,9], as well as decreasing its particle size down to nanometers [10–11]. Especially, Armand et al. found that a carbon coating $LiFePO_4$ synthesis simultaneously increases the electronic conductivity and prevents the growing particle, which is also a significant breakthrough for the applications of $LiFePO_4$ [3]. And after that, a lot of the surface modification technologies have been developed for enhancing the electrochemical performances of $LiFePO_4$ [12–15]. It is suggested that the purity of phase, the smaller particle size, uniformity of coating, reduced agglomeration and so on are significant for getting better electrochemical properties.

In order to understand the lithium intercalation/deintercalation mechanism, a two-phase reaction has been suggested [16–20], where there exist very narrow solid solutions in the vicinity of the end members $LiFePO_4$ and $FePO_4$. Moreover, Chen et al. confirmed the easy diffusion of lithium in the tunnels parallel to the *b* direction and found that lithium is extracted at the phase boundary parallel to the *bc* plane that progresses in the *a* direction on reaction [21]. By X-ray diffraction and electron microscopy, Delmas et al. found the coexistence of fully intercalated and fully deintercalated individual particles [20]. On this basis, a reaction mechanism with 'domino-cascade model' was constructed, which is hoped to try to understand the dynamics processes involved in electrochemical cycling starting from $LiFePO_4$ nanoparticles.

The phase changes of $LiFePO_4$ in Li^+ intercalation/deintercalation have been studied by ensemble averaging methods including XRD [20], Mossbauer [17] and electrochemistry [22]. However, there exist limitations in observing the surface related properties of cathode material using these methods. Fortunately, Raman spectroscopy provides a more localized technology to study the surface phase change and microstructures during charge and discharge [23]. By Raman spectroscopy, they found the incomplete delithiation of large $LiFePO_4$ due to the 1D channel blocking with anti-site defects. In Raman studies of $LiFePO_4$, both internal and external modes were suggested. In the internal modes, the very sharp band at 951 cm^{-1} is attributed to the Ag mode of ν_1, while the two weaker bands at 995 and 1067 cm^{-1} are thought to belong to the antisymmetric stretching modes of the PO_4^{3-} anion (ν_3). These three peaks at 953, 995 and 1067 cm^{-1} are considered to be characteristic for $LiFePO_4$. In the external modes, the peaks at 175 cm^{-1}, 244 cm^{-1} and 305 cm^{-1} correspond to translation of Fe,

* Corresponding author at: Fujian Provincial Key Laboratory of Quantum Manipulation and New Energy Materials, College of Physics and Energy, Fujian Normal University, Fuzhou 350117, China.
E-mail address: zghuang@fjnu.edu.cn (Z. Huang).

http://dx.doi.org/10.1016/j.ssi.2016.05.017
0167-2738/

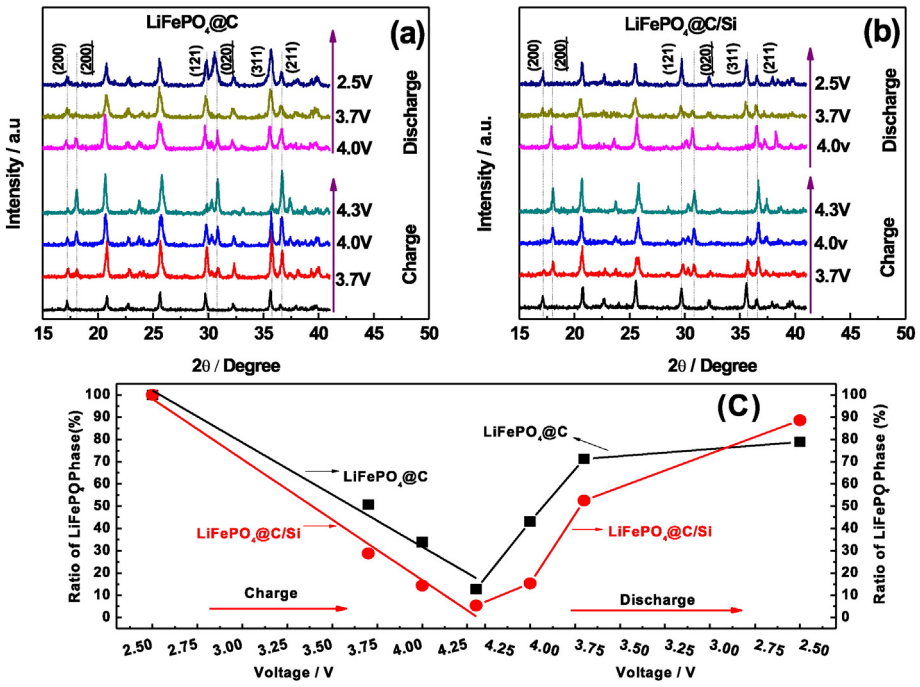

Fig. 1. XRD patterns of (a) $LiFePO_4$@C and (b) $LiFePO_4$@C/Si galvanostatically charged to $V_c = 3.7$ V, 4.0 V and 4.3 V at 2C rate, then kept at this voltage until the current was less than 0.2C, and galvanostatically discharged down to $V_{dc} = 4.0$ V, 3.7 V and 2.5 V at 2C rate respectively. (c) The graphic of $LiFePO_4$ phase as a function of voltage.

coupled translation of Fe and PO_4^{3-}, which indicates a phase change from $LiFePO_4$ to $FePO_4$. Additionally, Bai et al. still observedα-Fe_2O_3 phase with Raman peaks of 211 and 279 cm^{-1} in the thermal effect of pure, C-coated and Co-doped $LiFePO_4$ [24].

To our knowledge, the dynamics processes of $LiFePO_4$ phase change upon Li^+ extraction and insertion have been performed largely by XRD, Raman spectroscopy. However, the influence of the surface modification on the dynamics processes of $LiFePO_4$ phase change has hardly been studied. In this letter, Li^+ ion kinetic processes of $LiFePO_4$@C and $LiFePO_4$@C/Si electrodes are systematically investigated by X-ray diffraction, Raman spectra and Electrochemical impedance spectroscopy (EIS), respectively. The experimental results indicate that $LiFePO_4$@C/Si has faster charged and discharged velocity than $LiFePO_4$@C. Moreover, it is found that the nano silicon surface modification induces the lower activation energy of Li ions diffusion, which promotes Li^+ ion transfer rate. At last, it is observed that the nano silicon modification suppresses effectively the Fe dissolution and enhances the stability of $LiFePO_4$ phase and cycle performance.

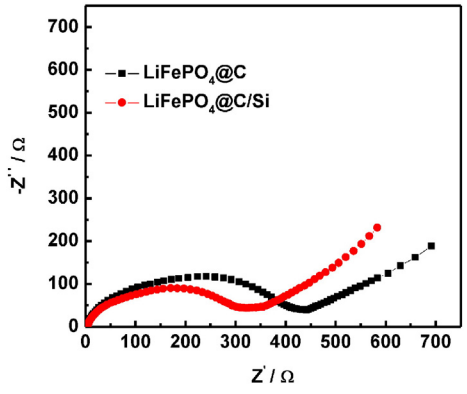

Fig. 2. The typical nyquist plots of $LiFePO_4$@C and $LiFePO_4$@C/Si in the fully discharge state after 1 cycle at 2C rate.

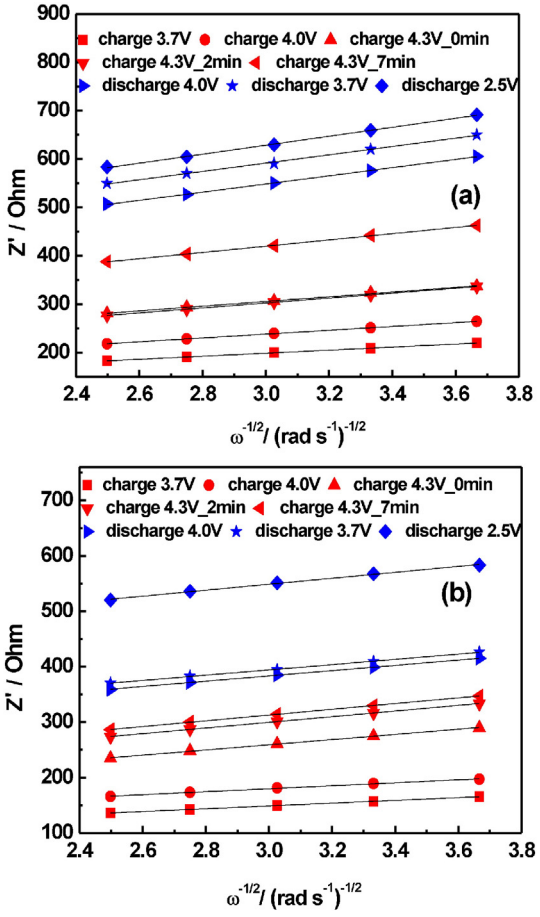

Fig. 3. Z′ vs. $\omega^{-1/2}$ plots in the low frequency of (a) $LiFePO_4$@C and (b) $LiFePO_4$@C/Si.

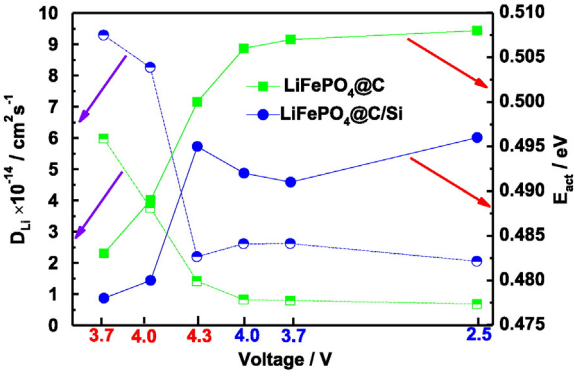

Fig. 4. The diffusion coefficient and activation energy of Li ion as a function of charge and discharge voltage for $LiFePO_4$@C and $LiFePO_4$@C/Si.

2. Experimental

$LiFePO_4$@C electrodes were prepared by pasting a slurry consisting of 80 wt.% commercial active material, 10 wt.% super-P and 10 wt.% polyvinylidene fluoride dissolved in *N*-methy1–2-pyrrolidone on an aluminum foil and dried at 110 °C overnight under vacuum. Moreover, detailed preparation of nano silicon modifying $LiFePO_4$@C electrodes could be found in our previous work [25]. Afterwards, the electrodes were punched into 12.5 mm diameter circular disk and assembled into the coin cells (R2025) with lithium metal as anode, Celgard 2300 microporous polyethylene membrane as separator and 1 M $LiPF_6$ in a mixture of ethyl carbonate (EC) and dimethyl carbonate (DMC) (1:1 in vol. ratio) as electrolyte in an argon-filled glove box.

In the charging process, $LiFePO_4$@C and $LiFePO_4$@C/Si were galvanostatically charged to $V_c = 3.7$ V, 4.0 V and 4.3 V at 2C rate (1C = 170 mA·h/g) respectively, then kept at this voltage until the current was less than 0.2C (34 mA·h/g). In the discharging process, $LiFePO_4$@C and $LiFePO_4$@C/Si cells full charged galvanostatically were discharged down to $V_{dc} = 4.0$ V, 3.7 V and 2.5 V at 2C rate, respectively. Moreover, to study the influence of the surface modification on the dynamics processes of $LiFePO_4$ phase change, another charged strategy was considered as following: $LiFePO_4$@C and $LiFePO_4$@C/Si cells were galvanostatically charged to 4.3 V at 2C rate, subsequently they were charged at 4.3 V (constant voltage). In this constant voltage process, three charged times with 0.0 min, 2.0 min and 7.0 min were chosen, respectively. Eventually, the above coin cells at different condition were disassembled and washed by propylene carbonate in an argon-filled glove box.

The charge/discharge measurements were conducted with a CT2001A cell test instrument (LAND Electronic Co.). The electrochemical impedance spectra (EIS) were performed by electrochemical workstation (CHI660C). The $LiFePO_4$@C and $LiFePO_4$@C/Si electrodes were measured using an X-ray (XRD, Rigaku MiniFlex II) with CuK_α radiation ($\lambda = 0.15405$ nm). The Raman spectra were recorded at room temperature using HORIBA Jobin Yvon Evolution by the assistance of a 50× long working distance objective with laser excitation at 532 nm, of which the total power was adjusted below 5 mW. The surface

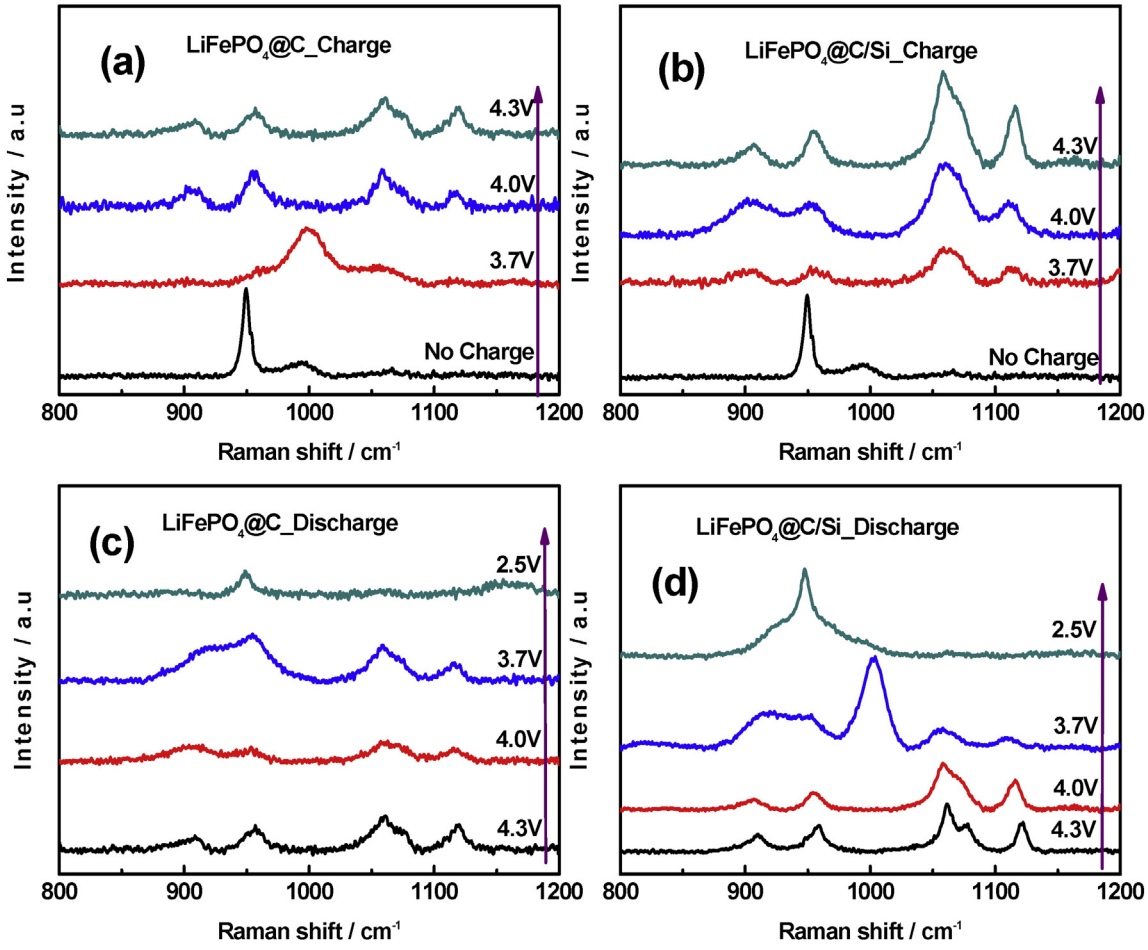

Fig. 5. The Raman spectra of (a) $LiFePO_4$@C and (b) $LiFePO_4$@C/Si corresponding the experimental conditions in Fig. 1.

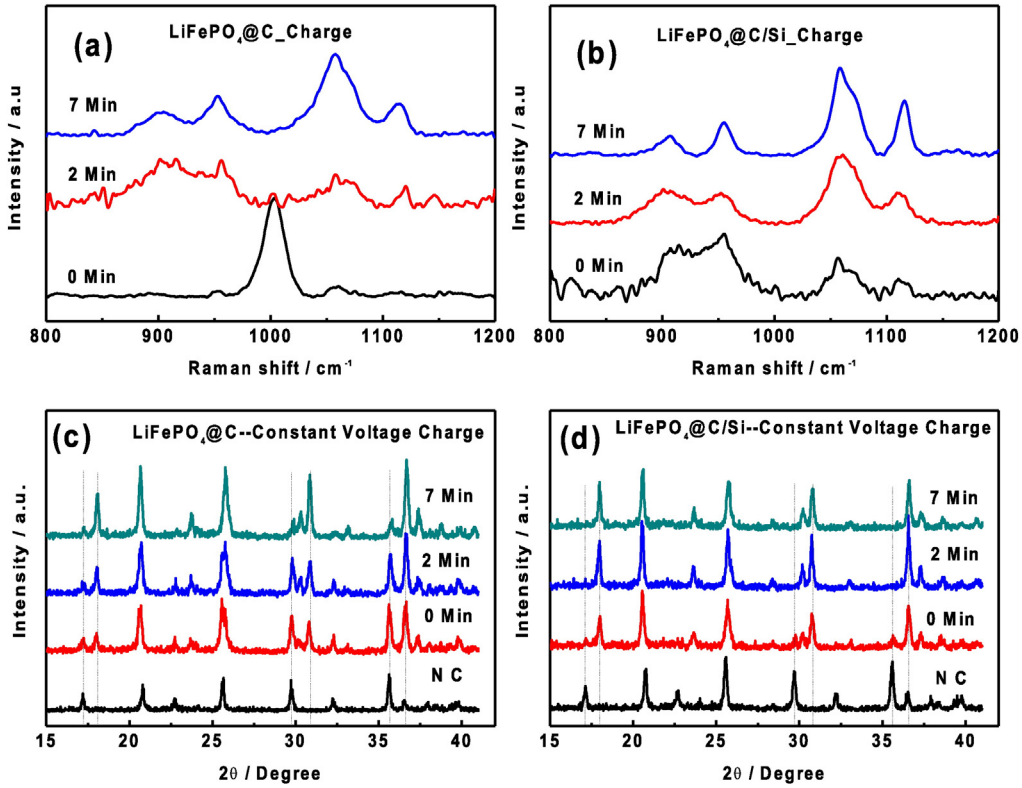

Fig. 6. The Raman spectra of (a) $LiFePO_4$@C and (b) $LiFePO_4$@C/Si at $T_{4.3V} = 0.0$ min, 2.0 min and 7.0 min; XRD patterns of (c) $LiFePO_4$@C and (d) $LiFePO_4$@C/Si at $T_{4.3V} = 0.0$ min, 2.0 min and 7.0 min.

morphologies of $LiFePO_4$ electrodes experienced several cycles were detected by a scanning electron microscope (SEM, Hitachi SU8010).

3. Results and discussion

XRD patterns of $LiFePO_4$@C and $LiFePO_4$@C/Si with different charge and discharge voltage conditions are present in Fig. 1(a) and (b), respectively. From the figures, it is found that the diffraction peaks (200), (020) located at $2\theta = 17.9°$, 30.7°are characteristic, which can be identified as the $FePO_4$ phases [20,21]. And the peaks (200), (121) and (311) around at 17.1°, 29.6° as well as 35.6° are characterized as $LiFePO_4$ phase. On the changed process for $LiFePO_4$, as the voltage increases, the intensities of peaks at 17.9°and 30.7°gradually increase while those of the peaks at 17.1°, 29.6°and 35.6°are reduced step by step, which means the gradually performed phase transformation between $LiFePO_4$ and $FePO_4$. When the transformation from triphylite phase to heterosite phase was completed, the peaks at 17.1° and 29.6° belonging to characteristic ones of $LiFePO_4$ vanished. Obviously, it can be observed that the intensity of diffraction peaks in discharge process has the opposite change rule relative to that in the charging process. The changed results of above characteristic peaks are agreed well with the diffractograms of a chemical delithiation research of $LiFePO_4$ [10,20]. At the same time, it is considered that the intensity changes of characteristic peaks belonging to $LiFePO_4$ and $FePO_4$ present the dynamics processes of Li^+ extraction and insertion. Moreover, compared to $LiFePO_4$@C electrode, $LiFePO_4$@C/Si electrode displays quite different phase transformation process. The area ratio of both peaks located at 17.1 ° (characteristic (200) for $LiFePO_4$) and 17.6 ° (characteristic (200) for $FePO_4$) is simply considered to be as the ratio of both phases ($LiFePO_4$ and $FePO_4$). Fig. 1(c) shows the ratio of $LiFePO_4$ phase as functions of charged and discharged voltages for $LiFePO_4$@C and $LiFePO_4$@C/Si. From the figure, it is found that the surface modification of nano silicon influences evidently the depth of charge, the velocity of charge and discharge. Clearly, $LiFePO_4$@C/Si electrode may possess faster Li^+ ion migration rate than $LiFePO_4$@C electrode. Moreover, from the slope of the ratio to charged and discharged voltages, $LiFePO_4$@C/Si electrode has faster charged and discharged speed than $LiFePO_4$@C, which means that the nano silicon on the surface induces the lower activation energy of Li ion diffusion.

In order to prove further the results above, EIS tests were applied to measure the Li^+ diffusion coefficient and investigate the Li^+ dynamics processes of $LiFePO_4$ electrode [16,26–27]. Fig. 2 shows the typical Nyquist plots of $LiFePO_4$@C and $LiFePO_4$@C/Si after 1 cycle at 2C rate. Here, an intercept at the Z′ axis in the high frequency represents the resistance of the electrolyte (R_s); The semicircle in the middle frequency range indicates the charge transfer resistance (R_{ct}); The inclined line in the low frequency stands for the Warburg impedance (W), which is associated with the solid-state diffusion of lithium ion inside active material. According to the plots in the low-frequency region, the diffusion coefficient (D_{Li}) of lithium ion could be calculated by the following equations [26,27],

$$Z\prime = R_{ct} + R_s + \sigma\omega^{-1/2} \tag{1}$$

$$D_{Li} = \frac{R^2T^2}{2A^2n^4F^4C_{Li}^2\sigma^2} \tag{2}$$

where the meaning of R is the gas constant, T the absolute temperature, n the number of electrons per molecule, A the surface area, F the Faraday constant, C_{Li} the concentration of lithium ion, ω the angular frequency, and σ is the Warburg factor which is relationship with Z'. The Z'-$\omega^{-1/2}$ plots for various charge and discharge voltage states of $LiFePO_4$@C and LiFePO4@C/Si are presented in Fig. 3(a) and (b), respectively. The lithium ion diffusion coefficient at different charge and discharge voltage condition are calculated according to Eqs. (1) and (2). Moreover, the activation energy for lithium ion diffusion can be calculated by the following

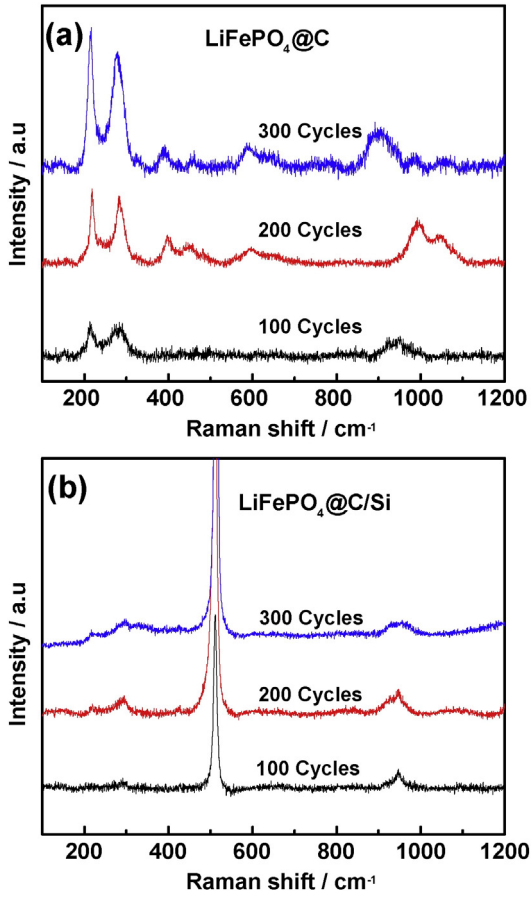

Fig. 7. The Raman spectra of (a) $LiFePO_4$@C and (b) $LiFePO_4$@C/Si at 2C rate after 100, 200, 300 cycles.

equation [28],

$$D_{Li} = a^2 \upsilon \exp(E_{act}/k_B T) \quad (3)$$

where a is approximately 3 Å, corresponding to the distance of a hop along the [010] direction, υ is about 10^{13} Hz, which is generally in the range of phonon frequencies, k_B is Boltzmann constant and T is the absolute temperature. Fig. 4 shows the diffusion coefficient and activation energy of Li ion as a function of charge and discharge voltage for $LiFePO_4$@C and $LiFePO_4$@C/Si, respectively. From the figure, it is found that, $LiFePO_4$@C/Si possesses larger diffusion coefficient and less activation energy than $LiFePO_4$@C, which means that the nano silicon surface modification enhances Li^+ ion migration rate. Here, the silicon on the surface induces the lower activation energy of Li ion diffusion, which is similar to the reducing activation energy reduced by sulfur surface modification [29]. The above results are consistent with the increase of charge depth, the enhancing charge and discharge velocity, as seen in Fig. 1.

To get insight into the effect of nano silicon on the surface of $LiFePO_4$ electrode, Raman spectroscopy was applied to study the surface structures by the vibrational properties of electrode materials as the charged and discharged voltages increase or decrease gradually. Raman spectra of $LiFePO_4$@C and $LiFePO_4$@C/Si during charging-discharging processes are shown in Fig. 5(a),(b),(c) and (d), respectively. As shown in Fig. 5, it is found that the peak at 951 cm^{-1} accompanying with weak asymmetric stretching peaks at 995 cm^{-1} and 1067 cm^{-1} displays pure $LiFePO_4$ phase for no-charged $LiFePO_4$@C and $LiFePO_4$@C/Si [23,24]. The stretching modes at 908, 960, 1068 and 1126 cm^{-1} should correspond to $FePO_4$ phase. In the charged process, as the voltage is enhanced to 3.7 V, the main $FePO_4$ phase has been observed on the surface of $LiFePO_4$@C/Si. Moreover, as the voltage is further enhanced to 4.0 and

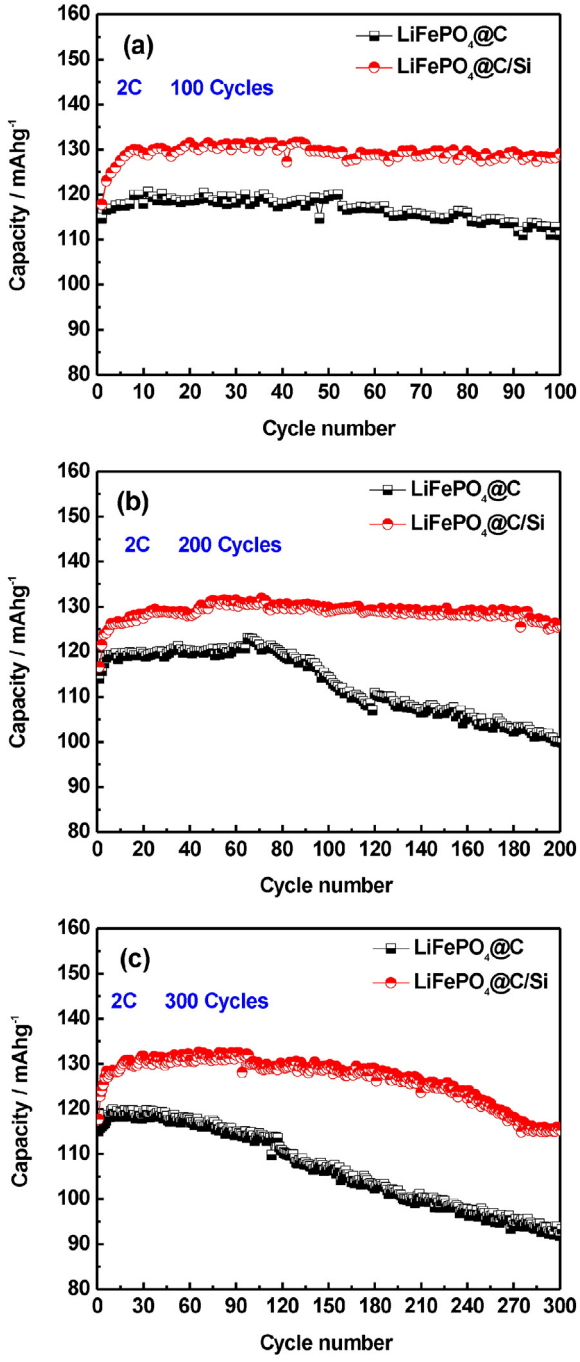

Fig. 8. Cycle performances of $LiFePO_4$@C and $LiFePO_4$@C/Si with (a) 100, (b) 200 and (c) 300 cycles at 2C rate.

4.3 V, the four peaks at 908, 960, 1068 and 1126 cm^{-1} become more and more acute. However, for $LiFePO_4$@C, the strong peak at 995 cm^{-1} accompanying with weak peaks at 908, 960, 1068 and 1126 cm^{-1} is observed as the voltage is enhanced to 3.7 V, which means that the main phase is still $LiFePO_4$. At the same time, as the voltage is further enhanced to 4.0 and 4.3 V, the sharpness of four peaks at 908, 960, 1068 and 1126 cm^{-1} for $LiFePO_4$@C is lower than that for $LiFePO_4$@C/Si. Similar results can be observed in the discharged processes as the voltage is reduced from 4.3 V to 2.5 V. In short, the nano silicon modification induces faster phase transformation between $LiFePO_4$ and $FePO_4$. That is, it induces faster Li^+ ion diffusion velocity, which is consistent with the above measured results by XRD and EIS.

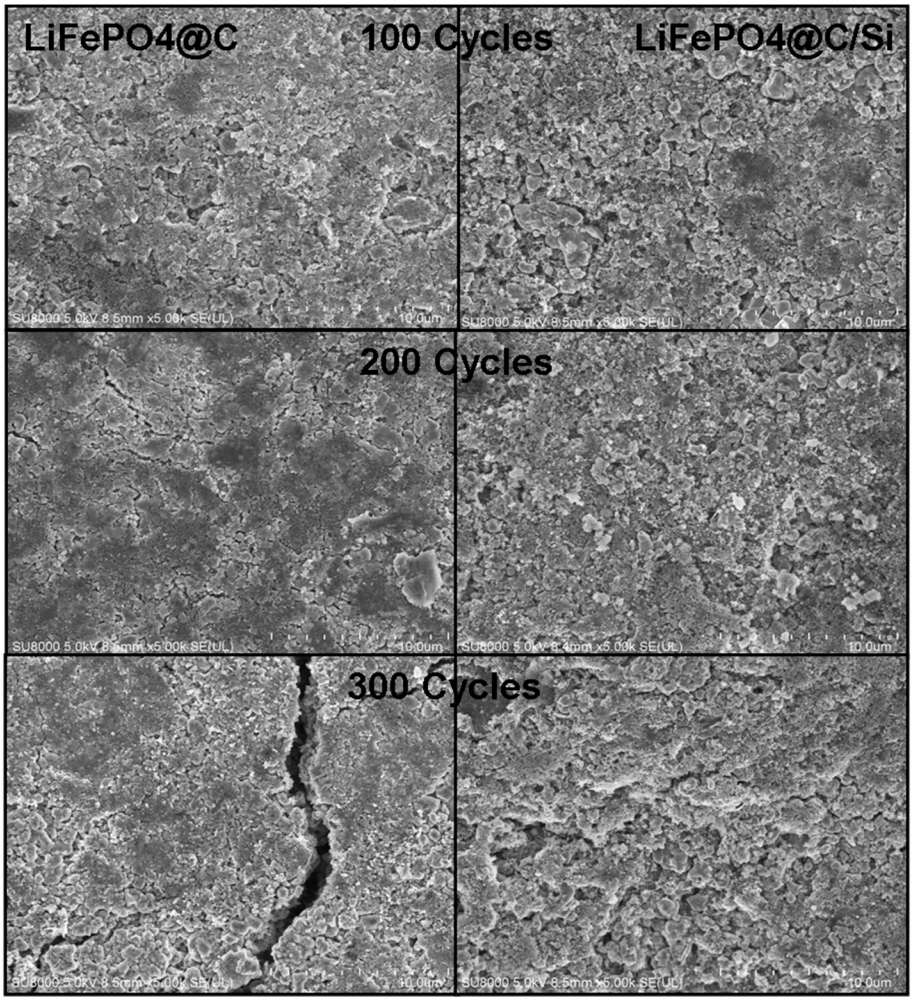

Fig. 9. SEM images of (a) $LiFePO_4$@C and (b) $LiFePO_4$@C/Si at 2C rate after 100, 200, 300 cycles.

To study Li^+ kinetic process of $LiFePO_4$ electrode in constant-voltage charged process, $LiFePO_4$@C and $LiFePO_4$@C/Si cells were galvanostatically charged to 4.3 V at 2C rate, subsequently they were charged at 4.3 V (constant voltage) with $T_{4.3V} = 0.0$ min, 2.0 min and 7.0 min, respectively. Figs. 6(a),(b) and (c),(d) show Raman spectra and XRD patterns of $LiFePO_4$@C and $LiFePO_4$@C/Si with three charged times, respectively. From Fig. 6(a), it is found that, for $T_{4.3V} = 0.0$ min and $LiFePO_4$@C, the strong peak at 995 cm^{-1} accompanying with weak peaks at 960, 1068 and 1126 cm^{-1} are observed for $LiFePO_4$@C, which indicates that the main phase is still $LiFePO_4$ and the Li^+ deintercalation from the $LiFePO_4$@C electrode is slightly performed. As $T_{4.3V} = 2.0$ min, the bands at 908, 960, 1068 and 1126 cm^{-1} can be more clearly identified, signifying a main phase transformation from $LiFePO_4$ to $FePO_4$ on the surface of electrode. As $T_{4.3V} = 7.0$ min, the peaks at 908, 960, 1068 and 1126 cm^{-1} become evidently more sharp, indicating a complete phase transformation. However, for $LiFePO_4$@C/Si, as $T_{4.3V} = 0.0$ min, the peaks at 908, 960, 1068 and 1126 cm^{-1} have been clearly indentified, signifying faster phase transformation from $LiFePO_4$ to $FePO_4$ than $LiFePO_4$@C. The above Raman studies show mainly the structure change and Li^+ ion diffusion on the surface of the electrode. While their average information can also be measured by X-ray diffraction, as found in Fig. 6(c) and (d). For $LiFePO_4$@C, the ratios of $LiFePO_4$ phase for $T_{4.3V} = 0.0$ min, 2.0 min and 7.0 min are 42.9%, 36.2% and 12.7%, respectively. However, for $LiFePO_4$@C/Si, they are 20.1%, 8.7% and 4.2%, respectively. Clearly, XRD patterns and Raman spectra farther prove that Li^+ ion diffusion rate and the phase change speed of $LiFePO_4$@C cathode are promoted by the nano silicon surface modification. Additionally, from the above Raman and XRD experimental results, it is found that constant-voltage charge with some time is indispensable for a fully delithiation of the $LiFePO_4$ material.

The Raman spectra of $LiFePO_4$@C and $LiFePO_4$@C/Si at 2C rate after 100, 200, 300 cycles are presented in Fig. 7(a) and (b), respectively. For $LiFePO_4$@C, after 100 cycles at 2C, a broad peak at 951 cm^{-1} belonging to $LiFePO_4$ phase in the high wave number region is found. At the same time, the other both peaks at 225, 291 cm^{-1} are observed, which is considered as the characteristic spectra of α-Fe_2O_3 clusters [24]. When the cycle number reach up to 200, the peak located at 951 cm^{-1} disappears while two new characteristic peaks at 995, 1067 cm^{-1} corresponding to asymmetric stretching of PO_4^{3-} anion appear. Simultaneously, the intensity of α-Fe_2O_3 characteristic peaks at 225, 291 cm^{-1} is further enhanced. As 300 cycle number is achieved, the modes at 995, 1067 cm^{-1} disappear quickly. Instead, the new mode at 908 cm^{-1} belonging to $FePO_4$ phase emerges in the high wave number region, and the intensity of peaks corresponding α-Fe_2O_3 phase becomes very sharp. On the contrary, for LiFePO4@C/Si after 100 cycles at 2C, there is no existence of other phases such as α-Fe_2O_3 and $FePO_4$, except for the characteristic sharp peak at 951 cm^{-1} of $LiFePO_4$ and representative peak of silicon [25,30,31]. Although the weak peaks at 225, 291 cm^{-1} belong toα-Fe_2O_3 phase could be found for 200 and 300 cycle number, the broader peak at 951 cm^{-1} still remains well. The above Raman spectra experiments mean that the nano silicon modification suppresses effectively the Fe dissolution and enhances the stability of $LiFePO_4$ phase, which is associated with the

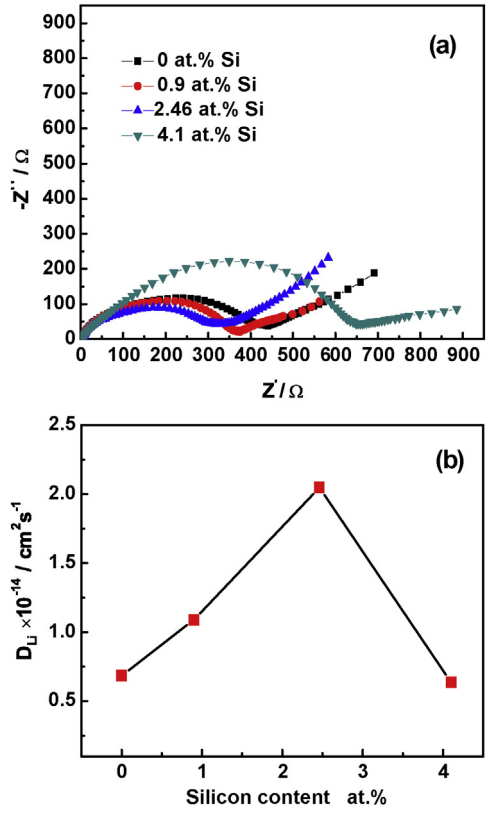

Fig. 10. (a) The typical impedance spectra of $LiFePO_4$@C modified various content silicon in the fully discharge state after 1 cycle at 2C rate. (b) The Li ion diffusion coefficient as a function of silicon modified content.

evident improvement of the cycle performance, as seen in Fig. 8. Fig. 8 shows the cycle performances of $LiFePO_4$@C and $LiFePO_4$@C/Si with 100, 200 and 300 cycles at 2C rate. From the figure, it is evidently that the nano silicon modification improves well the cycle performances. It is also proved by the cracking degree of $LiFePO_4$@C and $LiFePO_4$@C/Si at 2C rate after 100, 200, 300 cycles, as shown in Fig. 9. Fig. 9 shows SEM images of $LiFePO_4$@C and $LiFePO_4$@C/Si at 2C rate after 100, 200, 300 cycles. From the figure, it is clearly seen that the cracking degree is reduced by the silicon surface modification.

At last, the effect of the different content of nano silicon surface modification on Li^+ dynamics processes of $LiFePO_4$ is investigated by EIS. Fig. 10(a) and (b) show the Nyquist plots of $LiFePO_4$@C/Si with various silicon content after 1 cycle, and the Li ion diffusion coefficient as a function of silicon modified content, respectively. From the figure, it is clearly observed that $LiFePO_4$@C/Si (Si content = 2.46 at.%) displays lowest R_{ct} and largest Li^+ diffusion coefficient in four samples, which means that there exists the best silicon surface modification content in enhancing the electrochemical performances of $LiFePO_4$@C.

4. Conclusions

Both charged or discharged processes were considered. One: $LiFePO_4$@C and $LiFePO_4$@C/Si were galvanostatically charged or discharged to some V_c value at 2C rate, then kept at this voltage until the current was less than 0.2C; Another: $LiFePO_4$@C and $LiFePO_4$@C/Si cells were galvanostatically charged to some V_c value at 2C rate, subsequently they were charged at constant voltage, then three charged times with 0.0 min, 2.0 min and 7.0 min were chosen. Moreover, the phase changes of $LiFePO_4$@C and $LiFePO_4$@C/Si electrodes in Li^+ intercalation/deintercalation are systematically studied by XRD, Raman and EIS, respectively. The experimental results indicate that $LiFePO_4$@C/Si has faster charged and discharged velocity than $LiFePO_4$@C. Moreover, it is found that, $LiFePO_4$@C/Si possesses larger diffusion coefficient and less activation energy than $LiFePO_4$@C, which is consistent with the increase of charge depth, the enhancing charge and discharge velocity. At the same time, it also suppresses effectively the Fe dissolution. And it is observed that there exists the best silicon content in enhancing the electrochemical performances of $LiFePO_4$@C through EIS measurement. At last, it is suggested that constant-voltage charge is indispensable for a fully delithiation of the $LiFePO_4$ material.

Acknowledgment

We acknowledge the financial support by National Fundamental Research Program of China (Grant No. 2011CBA00200), the National Natural Science Foundations of China (No. 61574037, No. 21203025, No. 11344008, No. 11204038), Science and Technology Major Projects of Fujian Province (2013HZ0003), Project of Fujian Development and Reform Commission (2013-577) and Educational Department of Fujian Province (JK201310, JA13064).

References

[1] A.K. Padhi, K.S. Nanjundaswamy, J.B. Goodenough, J. Electrochem. Soc. 144 (1997) 1188–1194.
[2] A.K. Padhi, K.S. Nanjundaswany, C. Masquelier, S. Okada, J.B. Goodenough, J. Electrochem. Soc. 144 (1997) 1609–1613.
[3] N. Ravet, et al., Electrode material having improved surface conductivity, 2016 CA Patent No. EP1049182 (2000-05-02 2002), 2012.
[4] X.-L. Wu, L.-Y. Jiang, F.-F. Cao, Y.-G. Guo, L.-J. Wan, Adv. Mater. 21 (2009) 2710–2714.
[5] F. Yu, S.H. Lim, Y. Zhen, Y. An, J. Lin, J. Power Sources 271 (2014) 223–230.
[6] Z.P. Ma, Y.S. Peng, G.L. Wang, Y.Q. Fan, J.J. Song, T.T. Liu, X.J. Qin, G.J. Shao, Electrochem. Acta 156 (2015) 9077–9085.
[7] Z.P. Ma, G.J. Shao, X.J. Qin, Y.Q. Fan, G.L. Wang, J.J. Song, T.T. Liu, J. Power Sources 269 (2014) 194–202.
[8] R. Trocoli, S. Franger, M. Cruz, J. Morales, J. Santos-Pena, Electrochem. Acta 135 (2014) 558–567.
[9] M. Talebi-Esfandarani, O. Savadogo, Solid State Ionics 261 (2014) 81–86.
[10] G.L. Huang, W. Li, H.Z. Sun, J.W. Wang, J.P. Zhang, H.X. Jiang, F. Zhai, Electrochem. Acta 97 (2013) 92–98.
[11] K. Vediappan, A. Guerfi, V. Gariépy, G.P. Demopoulos, P. Hovington, J. Trottier, A. Mauger, C.M. Julien, K. Zaghib, J.Power Sources 226 (2014) 99–106.
[12] Y.B. Lin, Y. Lin, T. Zhou, G.Y. Zhao, Y.D. Huang, Z.G. Huang, J. Power Sources 226 (2013) 20–26.
[13] K.-S. Park, P. Xiao, S.-Y. Kim, A. Dylla, Y.-M. Choi, G. Henkelman, K.J. Stevenson, J.B. Goodenough, Chem. Mater. 24 (2012) 3212–3218.
[14] K. Bazzi, B.P. Mandal, M. Nazri, V.M. Naik, V.K. Garg, A.C. Oliveira, P.P. Vaishnava, G.A. Nazri, R. Naik, J. Power Sources 265 (2014) 67–74.
[15] H.W. Tang, Y.L. Si, K. Chang, F. Xiaoning, L. Bao, E. Shangguan, Z. Chang, X.-Z. Yuan, H.J. Wang, J. Power Sources 295 (2015) 131–138.
[16] R. Malik, A. Abdellahi, G. Ceder, J. Electrochem. Soc. 160 (2013) A3179–A3197.
[17] A.S. Andersson, B. Kalska, L. Haggstrom, J.O. Thomas, Solid State Ion. 130 (2000) 41–52.
[18] A. Yamada, H. Koizumi, N. Sonoyama, R. Kanno, Electrochem, Solid State Lett. 8 (2005) A409–A413.
[19] Y.H. Kao, M. Tang, N. Meethong, J. Bai, W.C. Carter, C. Yet-Ming, Chem. Mater. 22 (2010) 5845–5855.
[20] C. Delmas, M. Maccario, L. Croguennec, F. Le Cras, F. Weill, Nat. Mater. 7 (2008) 665–671.
[21] G.Y. Chen, X.Y. Song, T.J. Richardson, Electrochem. Solid State Lett. 9 (2006) A295–A298.
[22] H. Matsui, T. Nakamura, Y. Kobayashi, M. Tabuchi, Y. Yamada, J. Power Sources 195 (2010) 6879–6883.
[23] J. Wu, G.K.P. Dathar, C.W. Sun, M.G. Theivanayagam, D. Applestone, A.G. Dylla, A. Manthiram, G. Henkelman, J.B. Goodenough, K.J. Stevenson, Nanotechnology 24 (2013) 424009 (9pp).
[24] Y. Bai, Y.F. Yin, J.M. Yang, C.B. Qing, W. Zhang, J. Raman Spectrosc. 42 (2011) 831–838.
[25] W.Y. Yang, Z.Y. Zhuang, X. Chen, M.Z. Zou, G.Y. Zhao, Q. Feng, J.X. Li, Y.B. Lin, Z.G. Huang, Appl.Surf.Sci. 359 (2015) 875–882.
[26] J. Li, L. Zhang, L.F. Zhang, W.W. Hao, H.B. Wang, Q.T. Qu, H.H. Zheng, J. Power Sources 249 (2014) 311–319.
[27] H. Liu, C. Li, H.P. Zhang, L.J. Fu, Y.P. Wu, H.Q. Wu, J. Power Sources 159 (2006) 717–720.
[28] G.G. Xu, K.H. Zhong, J.M. Zhang, Z.G. Huang, Solid State Ionics 281 (2015) 1–5.
[29] G.G. Xu, K.H. Zhong, J.-M. Zhang, Z.G. Huang, J. Appl. Phys. 116 (2014) (063703-1-6).
[30] W. Xu, H.C. Sun, J. Xu, W. Li, W.W. Mu, Y. Liu, M.Y. Yan, X.F. Huang, K.J. Chen, Appl. Sur. Sci. 258 (2011) 346–349.
[31] S. Huet, G. Viera, L. Boufendi, Thin Solid Films 193 (2002) 403–404.